Acta Mech. Sin. (2011) 27(5):627–635
DOI 10.1007/s10409-011-0495-z

RESEARCH PAPER

Experimental and numerical studies of micro PEM fuel cell

Rong-Gui Peng · Chen-Chung Chung · Chiun-Hsun Chen

Received: 2 September 2009 / Revised: 13 June 2010 / Accepted: 29 October 2010

Abstract A single micro proton exchange membrane fuel cell (PEMFC) has been produced using Micro-electro-mechanical systems (MEMS) technology with the active area of 2.5 cm^2 and channel depth of about 500 μm. A theoretical analysis is performed in this study for a novel MEMS-based design of a micro PEMFC. The model consists of the conservation equations of mass, momentum, species and electric current in a fully integrated finite-volume solver using the CFD-ACE+ commercial code. The polarization curves of simulation are well correlated with experimental data. Three-dimensional simulations are carried out to treat prediction and analysis of micro PEMFC temperature, current density and water distributions in two different fuel flow rates (15 cm^3/min and 40 cm^3/min). Simulation results show that temperature distribution within the micro PEMFC is affected by water distribution in the membrane and indicate that low and uniform temperature distribution in the membrane at low fuel flow rates leads to increased membrane water distribution and obtains superior micro PEMFC current density distribution under 0.4 V operating voltage. Model predictions are well within those known for experimental mechanism phenomena.

Keywords Micro PEMFC · MEMS · Simulation · Fuel flow rate

Nomenclature

A	The x-dir. position in channel (m)
B	The y-dir. position in channel (m)
c_{ref}	Reference molar concentration (kmol·m^{-3})
$c_{\mathrm{C}}^{\mathrm{R}}$	Molar concentration of hydrogen in catalyst layer (kmol·m^{-3})
$c_{\mathrm{L}}^{\mathrm{R}}$	Molar concentration of hydrogen in channel (kmol·m^{-3})
D_{eff}	Gas effective diffusivity (m^2·s^{-1})
D	Diffusivity (m^2·s^{-1})
F	Faraday constant (C·$kmol^{-1}$)
H_{C}	Flow channel height (m)
H_{G}	GDL thickness (m)
h	Mixture enthalpy (J·kg^{-1})
$J_{\mathrm{C}}^{\mathrm{conv}}$	The mass flow rate from channels to GDL (kg·s^{-1})
$J_{\mathrm{G}}^{\mathrm{diff}}$	The mass flow rate from GDL to catalyst layer (kg·s^{-1})
j	Net current density (A·m^{-2})
j_{e}	Exchange current density (A·m^{-2})
M	Molecular weight (kg·$kmol^{-1}$)
p	Absolute pressure (Pa)
q	Heat flux (J·m^{-2})
R	Universal gas constant (kJ·$kmol^{-1}$·K^{-1})
S	Surface area (m^2)
Sh	Sherwood number
T	Temperature (K)
U	Fluid velocity (m·s^{-1})
V	Volume (m^3)
Y	Fluid mass fraction

Greek symbols

α	Mass transfer coefficient
β	Kinetic constant
ε	Porosity
ρ	Fluid density (kg·m^{-3})
η	Overpotential (V)
κ	Permeability (m^2)
μ	Dynamics viscosity (kg·m^{-1}·s^{-1})
σ	Electrical conductivity (Ω^{-1}·m^{-1})
τ	Shear stress tensor (Pa)
τ	Tortuosity
ϕ	Concentration exponent
ω	Production rate of water (kg·m^{-3}·s^{-1})

R.-G. Peng (✉) · C.-C. Chung · C.-H. Chen
Department of Mechanical Engineering,
National Chiao Tung University,
Hsinchu, Taiwan, China
e-mail: b68411@ms25.hinet.net

Superscripts

conv	Convection
diff	Diffusion
K	Reaction kinetics
N	Nerst
R	Molar
tot	Total

Subscripts

an	Anode
C	Flow channel
ca	Cathode
con	Concentration loss
e	Exchange
eff	Effective value
G	GDL
in	Inlet
L	Catalyst layer

1 Introduction

The micro proton exchange membrane fuel cell (PEMFC) is expected to be a major source of portable electrical power because of its low-temperature operation, quick start-up, lightweight packing, small volume, and low pollution potential. Micro-electro- mechanical systems (MEMS) technology offers advantages in manufacturing micro-scale materials and is used to make miniaturized electronic devices. Consequently, micro PEMFCs can be fabricated using MEMS technology for portable electronic power applications. A silicon substrate is used as the major material for a flow field plate. This study focuses on both MEMS fabrication and numerical simulation, which employs a silicon-MEMS technology to manufacture flow channels for use in a single micro PEMFC, and developing a three-dimensional model to elucidate its electrochemical properties in the membrane.

Early in 2000, Lee et al. [1] used microfabrication techniques, such as deep silicon etching, photo masked electroplating, physical vapor deposition, anodic bonding, and spin coating, on a silicon wafer to create flow channels. They produced a milliwatt micro fuel cell using new techniques and materials that had a current density of 150 mA/cm^2. Meanwhile, Hsieh et al. [2] developed a new design and fabrication process for a micro fuel cell flow field plate with a cross section of 5 cm^2 and a thickness of 800 μm. The novel design had a reported power density of 25 mW/cm^2 at 0.65 V, and the results obtained from tests on this fuel cell indicated a reliable and stable power output at ambient temperatures. Hsieh et al. [3] used the SU-8 photoresist microfabrication process to fabricate micro PEMFC flow channels. Their work contributed to the low-cost mass-production of a small, flat single fuel cell with a power density of 30 mW/cm^2 at 0.35 V.

In 2006, Cha et al. [4] studied the transport phenomena on flow channels in the micro fuel cell. The channels were constructed using a structural photopolymer and had 500 μm, 100 μm, and 20 μm wide measures. The effects of the channel size and the gas diffusion layer thickness were then examined. It was found that a high pressure drop in very small channels improved the convection of air into the gas diffusion layer (GDL) and improved fuel cell performance at a low current density. The results signified that using a thin GDL improved the performance of the micro fuel cell. Hsieh et al. [5] investigated the operational parameters of a H_2/air micro PEMFC with different flow configurations using impedance spectroscopy. The work considered a range of operating parameters for the backpressure and cell temperature in order to determine how the flow configuration affects the performance of the micro fuel cells. Optimal operating conditions were adopted to test the micro PEMFC stack [6]. The results demonstrated that the effect of the operational parameters on stack performance is similar to that on a single micro PEMFC.

For fuel cells with small dimensions, the influence on the mass transport or electrical conductivity is significant. Chiang and Chu [7] found that the membrane electrical conductivity increased when the aspect ratio channel was low. Shimpalee and Van Zee [8] investigated how serpentine flow fields with different channels/rib cross-sectional areas affected performance and species distributions for both automotive and stationary conditions. The simulation results indicated that for a stationary condition, a narrow channel with a wide rib spacing improved performance; however, the opposite occurs when the automotive condition is applied. Matamoros and Bruggemann [9] adopted steady and three-dimensional models to determine the influence of geometric parameters on cell performance under different humidity conditions. According to their results, anode and cathode liquid water saturation may affect species transport and the polymer electrolyte water content. Thus, one must simultaneously calculate both water absorption and desorption via the polymer electrolyte and liquid water saturation in the anode and cathode porous media in order to obtain an actual view of the ohmic and concentration losses in PEMFC performance.

Shimpalee et al. [10] examined different channel path lengths to determine the impact of flow path length on the temperature and current density distributions on PEMFC performance. According to their results, local temperature, water content, and current density distributions become increasingly uniform under serpentine flow field designs with short path lengths or an increased number of channels. Liu et al. [11] developed an isothermal, steady-state, three-dimensional multi-component transport model for a PEMFC. Their results revealed the detailed distribution characteristics of oxygen concentration, local current density, and cathode activation overpotential at different current densities.

Most previous simulation papers dealt with PEMFC flow channel configurations or water and thermal issues.

However, there are few complete computational models that consider the electrochemical properties of micro PEMFCs. In this study, a number of simulations are carried out, without considering the two-phase flow effect, to compare with the corresponding experimental results. We concentrate on investigating the effects of two different fuel flow rates, 15 cm^3/min and 45 cm^3/min, on the polarization curve, temperature, current density, and water distribution in the membrane. Better understanding of the distributions of temperature, current density, and water content in the micro PEMFC can help to further improve its performance.

2 Model development

A micro PEMFC has several components. These include the end plate, the gasket, the GDL, the membrane electrode assembly (MEA), the flow field plate, and the current collector. Figure 1a schematically depicts the micro PEMFC. Figure 1b displays a single micro PEMFC that has been fabricated with all of the components.

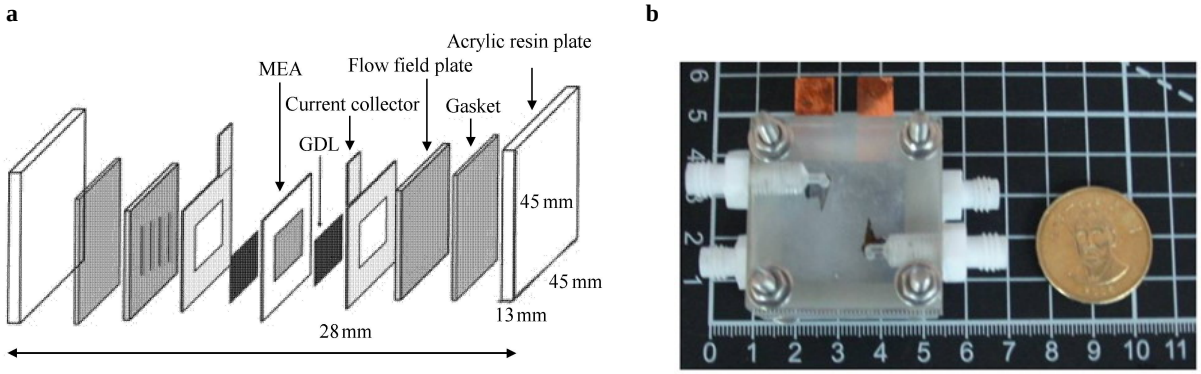

Fig. 1 **a** Scheme of micro PEMFC; **b** Picture of micro PEMFC

2.1 Basic assumptions

The following assumptions are utilized to simplify the simulation conditions for this study. The simulations performed are based on a steady state laminar flow, which neglects the effects of gravity. The gases are considered to behave like an ideal gas with a uniform distribution in the inlet. The flows in the catalyst layer, gas diffusion layer, and channel flow field are in the gaseous phase, and the effects of vaporization and condensation are not considered. The Butler–Volmer equation is used to describe the electrochemical reactions within the catalyst layer. The Nerst–Planck equation is used to describe the transport of protons through the membrane. The polarization curve is based on Ohm's law. The GDL, catalyst layer, and membrane are all isotropic porous media. The membrane is impermeable to gases and electrons. The physical transport properties are considered to be constant in each domain.

2.2 Governing equations

The three-dimensional mathematical model consists of the conservation equations of mass, momentum, species, and current in a fully integrated finite-volume solver using the CFD-ACE+ commercial code. The conservation equations used are listed below. Further details can be found in the work of Mazumder and Cole [12].

2.2.1 In the gas channel

Based on the above assumptions, the conservation equations of continuity, momentum, and species in the gas flow channel are follows:

Continuity equation

$$\frac{\partial \rho}{\partial t} + \nabla \cdot (\rho \boldsymbol{U}) = 0. \tag{1}$$

Momentum conservation equations:

X-axis

$$\frac{\partial \rho u}{\partial t} + \nabla \cdot (\rho \boldsymbol{U} u) = -\frac{\partial p}{\partial x} + \nabla \cdot (\mu \nabla u), \tag{2}$$

Y-axis

$$\frac{\partial \rho v}{\partial t} + \nabla \cdot (\rho \boldsymbol{U} v) = -\frac{\partial p}{\partial y} + \nabla \cdot (\mu \nabla v), \tag{3}$$

Z-axis

$$\frac{\partial \rho w}{\partial t} + \nabla \cdot (\rho \boldsymbol{U} w) = -\frac{\partial p}{\partial z} + \nabla \cdot (\mu \nabla w), \tag{4}$$

where ρ is the fluid density, p is the pressure, and μ is the dynamic viscosity.

Species conservation equation

$$\frac{\partial}{\partial t}(\rho Y_i) + \nabla \cdot (\rho \boldsymbol{U} Y_i) = \nabla \cdot J_i, \tag{5}$$

where Y_i is the mass fraction of the i-th species, and J_i is the diffusive flux.

The species diffusion flux may be written as

$$J_i = \rho D_i \nabla Y_i + \frac{\rho Y_i}{M} D_i \nabla M - \rho Y_i \sum_j D_j \nabla Y_j - \rho Y_i \frac{\Delta M}{M} \sum_j D_j Y_j, \quad (6)$$

where M is the mixture molecular weight, and D_i is the effective mass diffusion coefficient of species i. The first term represents the Fickian diffusion due to concentration gradients. The last three terms are correction terms necessary to satisfy the Stefan-Maxwell equations for multicomponent species i within the porous medium, and depend on the porosity, ε, and tortuosity, τ, of the medium

$$D_i = D_{i,FS} \varepsilon^{\tau}, \quad (7)$$

$D_{i,FS}$ is the free stream diffusion coefficient of the i-th species. It is common practice to use a tortuosity value of 1.5 in Eq. (7), resulting in the so-called Bruggeman model. The same value is adopted in the simulations due to lack of better information.

2.2.2 In the porous media

The continuity equation and momentum conservation equations are as follows

$$\frac{\partial}{\partial t}(\varepsilon\rho) + \nabla \cdot (\varepsilon\rho \boldsymbol{U}) = 0, \quad (8)$$

$$\frac{\partial}{\partial t}(\varepsilon\rho \boldsymbol{U}) + \nabla \cdot (\varepsilon\rho \boldsymbol{U}\boldsymbol{U}) = -\varepsilon \nabla p + \nabla \cdot (\varepsilon\tau) + \frac{\varepsilon^2 \mu \boldsymbol{U}}{\kappa}, \quad (9)$$

where ε is the porosity, ρ is the fluid density, $\boldsymbol{U}$ is the fluid velocity vector, p is the pressure, τ is the shear stress tensor, μ is the dynamic viscosity, and κ is the permeability (the square of effective volume to the surface area ratio of a porous medium). The last term in Eq. (9) represents Darcy's drag force imposed by the pore walls on the fluid, which leads to a significant pressure drop across the porous medium.

The species conservation equation is estimated as

$$\frac{\partial}{\partial t}(\varepsilon\rho Y_i) + \nabla \cdot (\varepsilon\rho \boldsymbol{U} Y_i) = \nabla \cdot J_i + \dot{\omega}_i, \quad (10)$$

where Y_i is the mass fraction of the i-th species, J_i is the mass diffusion flux of the i-th species, and $\dot{\omega}_i$ is the mass production rate of the i-th species in the gas phase. $\dot{\omega}_i$ is due to the heterogeneous electrochemical reactions within the porous media.

The temperature field of each domain is acquired by solving the energy conservation equation, which is written as follows

$$\nabla \cdot (\varepsilon\rho \boldsymbol{U} h) = \nabla \cdot q + \varepsilon\tau \cdot \nabla \boldsymbol{U} - j_e \left(\frac{S}{V}\right)_{\text{eff}} \eta + \frac{|j \cdot j|}{\sigma}, \quad (11)$$

where h is the gas enthalpy, q is the heat flux comprised of contributions due to thermal conduction, j_e is the exchange current density, S is the reaction surface area, V is the medium volume, η is the electrode over-potential, j is the transfer current density, and σ is the electrical conductivity.

Reactant species undergo electrochemical reactions at the electrode catalyst layers. Hydrogen is oxidized at the anode, and the corresponding proton is reduced at the cathode. These two reactions are driven by the potential difference, also called the activation over-potential, between the solid phase and the electrolyte phase. The Butler–Volmer equation, which describes this phenomenon, is expressed as

$$j = j_e \left(\frac{C}{C_{\text{ref}}}\right) \left[\exp\left(\frac{\beta_{\text{an}} F}{RT}\eta\right) - \exp\left(\frac{\beta_{\text{ca}} F}{RT}\eta\right) \right], \quad (12)$$

where C is the reactant molar concentration, C_{ref} is the reference molar concentration, β_{an} and β_{ca} are the kinetic constants determined from experimentally generated Tafel plots, and η is the over-potential between the solid and electrolyte phases of the electrode.

During the electrochemical reaction, the performance of the PEMFC drops when the reactant species concentrations are deficient on the reaction surfaces, especially when operating a PEMFC at a low operating voltage due to large amounts of water that can cause clogging. A concentration loss happens due to water clogging and bending channels. The total concentration loss is expressed as

$$\eta_{\text{con}}^{\text{ton}} = \frac{RT}{2F}\left(1 + \frac{1}{\alpha}\right) \ln \frac{C_{\text{C}}^{\text{R}}}{C_{\text{L}}^{\text{R}}}, \quad (13)$$

where C_{C}^{R} is the reactant molar concentration in flow channels, C_{L}^{R} is the reactant molar concentration in catalyst layers, and α is the mass transfer coefficient expressing how variations in electrical potential across reaction interfaces change the reaction rate. The value of α depends on the reaction and electrode material.

One concentration loss, called the Nerst potential change due to reactant species depletion in catalyst layers, has the following form

$$\eta_{\text{con}}^{\text{N}} = \frac{RT}{2F} \ln \frac{C_{\text{C}}^{\text{R}}}{C_{\text{L}}^{\text{R}}}. \quad (14)$$

The second form by which a concentration contributes to concentration loss is via reaction kinetics. It has the following form

$$\eta_{\text{con}}^{\text{K}} = \frac{RT}{2\alpha F} \ln \frac{C_{\text{C}}^{\text{R}}}{C_{\text{L}}^{\text{R}}}. \quad (15)$$

2.3 Boundary conditions

The governing equations for the present micro PEMFC model are elliptic and partial differential equations. Hence, boundary conditions are required for all boundaries in the computational domain. The temperature of the outer surfaces of flow patterns was maintained at 323 K. The conditions of the anode inlet included a temperature of 323 K and a pressure of 300 kPa with a 1.2 stoichiometric flow rate of 100 % H_2. The conditions of the cathode inlet included a temperature of 323 K and a pressure of 300 kPa with a 2.0 stoichiometric rate of 100 % O_2. Each outer surface of the flow pattern in the z-direction is assigned for a specific solid-phase overpotential. This value is set to zero on the anode side, and the total over-potential is set on the cathode side. A co-current flow direction is applied in this investigation.

2.4 Solution strategy

Simulations are solved using the commercial computational package CFD-ACE+. The results are regarded to be converged, since the normalized residual of each parameter (such as temperature, pressure, and gases velocity) is less than 10^{-4}. The physical and chemical properties of the membrane in this model are those determined by Mazumder and Cole [12]. The membrane permeability is 1.8×10^{-18}, the porosity is 0.28, and the tortuosity is 5. The diffusivity of gases is calculated using Stefan Maxwell equations with a Bruggeman correction applied to account for the porosity and tortuosity in the porous media GDL, catalyst layers, and membrane. Tables 1 and 2 show the dimensions and properties of the flow field plate, membrane, electrode material properties, and the initial operating conditions used in the numerical simulation. The component parameters and transport properties used in this study were obtained from Mazumder and Cole [12] and Springer et al. [13].

Table 1 Dimensions, properties and parameters for the numerical model

Channel length/mm	14
Channel width/mm	0.3
Channel depth/μm	500
Rib width/mm	0.7
Diffusion layer thickness/mm	0.4
Catalyst layer thickness/mm	
Anode	0.018
Cathode	0.026
Membrane thickness/mm	0.035
Total reaction area/cm^2	2.5
Effective diffusivity (Bruggeman model)	$\tau = 5$
For membrane Bruggeman model for diffusion and catalyst layer	$\tau = 1.5$
Membrane permeability/m^2	1.8×10^{-18}
Diffusion and catalyst layer permeability/m^2	1.76×10^{-11}
Membrane porosity	0.28
Diffusion and catalyst porosity	0.4
Air and fuel side pressure/Pa	3.03×10^5
Transfer coefficient (Tafel constants) at anode	0.5
Reference current density at anode $((A\cdot m^{-3})(m^3(kg\cdot mol\cdot H_2)^{-1})^{1/2})$	9.23×10^8
Transfer coefficients (Tafel constants) at cathode	1.5
Reference current density at cathode $((A\cdot m^{-3})(m^3(kg\cdot mol\cdot H_2)^{-1})^{1/2})$	1.05×10^6
Diffusion and catalyst layer conductivity/$(\Omega m)^{-1}$	53

Table 2 Operating conditions for the numerical model

H_2 at fuel inlet/$(cm^3\cdot min^{-1})$	15 and 40
Anode gas	100 % H_2
O_2 at fuel inlet/$(cm^3\cdot min^{-1})$	15 and 40
Cathode gas	100 % O_2
Operating pressure/Pa	1.01×10^5
Operating temperature/K	323

2.5 Experimental

A micro PEMFC is set up to obtain the polarization curves. The end plate is made of acrylic, and its size is 45 mm×45 mm×13 mm. The gasket isolates and prevents gas leakage; it is made of silica gel and has a thickness of 1 mm. The GDL used herein is a standard carbon paper (CARBEL CL GDL) with a thickness of 0.4 mm. The MEA (thickness: 0.035 mm, catalyst loading of the anode and cathode: 0.5 mg/cm^2 Pt) is a commercial product. The micro PEMFC reaction area is 2.5 cm^2.

Silicon is used as the material of the substrate in the anode and cathode flow field plates. The flow field plates are formed using MEMS technology. Figure 2 depicts the procedure for fabricating the silicon wafer. A 4-inch diameter silicon wafer is used as the substrate in the investigation.

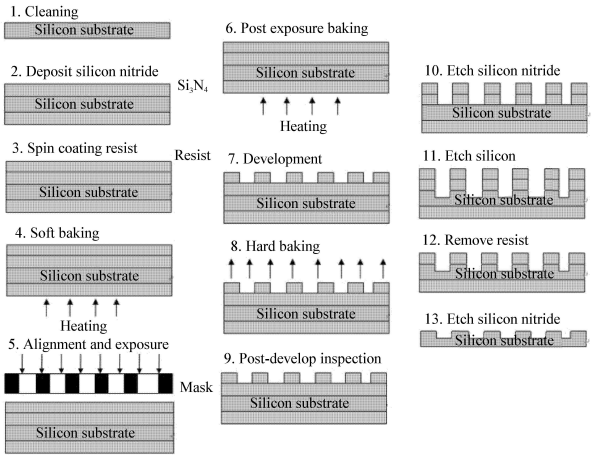

Fig. 2 Silicon wafer etching process

The contaminants on the surface of the silicon wafers at the start of the MEMS process or those that are accumulated in the middle of the process must be removed during processing. The purpose is to obtain high-performance and highly reliable semiconductor devices as well as diffusion and deposition tubes. It also serves to prevent equipment contamination, especially under a high temperature oxidation. Silicon wafers undergo Radio Corporation of America (RCA) cleaning as a standard procedure before they undergo high-temperature processing steps (i.e., oxidation, diffusion, and

chemical vapor deposition (CVD)) in semiconductor manufacturing.

A spinner is used to dry the wafer after RCA cleaning. Next, 200 nm silicon nitride is deposited by low-pressure chemical vapor deposition (LPCVD); one side of the silicon wafer is polished, and the silicon substrate is then spin-coated with a resistive layer 7 μm thick at various rotating speeds.

Next, the silicon substrate is soft baked. Soft baking is a process where almost all of the solvents are removed from the photoresist coating. Ultraviolet light with a g line is used for the exposure process. After exposure has been completed, heat is again applied for approximately 2–3 minutes for post exposure baking. Development is done in the vitrics to form micro flow channels.

The photoresist is hard-baked for about 1minute, and the silicon substrate is later examined development. The cavities of the flow structure are patterned by wet etching. Reactive ion etching (RIE) is conducted to etch a silicon nitride layer of 300 μm width. RIE is an etching technology that is used in microfabrication. It uses chemically reactive plasma to remove material that is deposited on wafers. Plasma is generated under low pressures in an electromagnetic field. The silicon nitride layer, however, was too thin to enable the fuel to flow from the inlet to the outlet. Hence, the exposed silicon wafer was etched to pattern micro PEMFC channels in an aqueous solution of 45% KOH at 80°C. The etching depth of the channel is 500 μm. The depth of the flow channels is expected to favor gas uniformity, water management, and reduced flow resistance. The resist is then removed from the silicon substrate. The final step employs phosphoric acid to remove the remaining silicon nitride at 180°C.

The shapes of the three serpentine channels, which have channel and rib widths of 0.3 mm and 0.7 mm, respectively, are used for both the anode and cathode flow fields. The channels are etched on the sides of the anode and cathode, and the depth of each channel is 500 μm. The holes for the feeding fuel are made by drilling from the rear side. The oversized flow field plates have an area of 2.5 cm^2, and a silicon wafer 4 inches in diameter is used to make four such flow field plates. Figure 3 shows the silicon substrate after etching.

Current collectors provide an electrical pad for electrical transmission to the external load. Unlike metal, the silicon wafer is not considered to be an ideal current collector material because of its high resistance. The silicon wafer is only used as a fuel carrier in this investigation. Therefore, the alternative design includes an MEA and GDL sandwiched between current collectors, which are made of brass foil. Consequently, the use of silicon substrates as flow field plates can be reduced since electrons do not pass through them. The advantage of this novel design is that no Au electroplate is required on top of the silicon wafer.

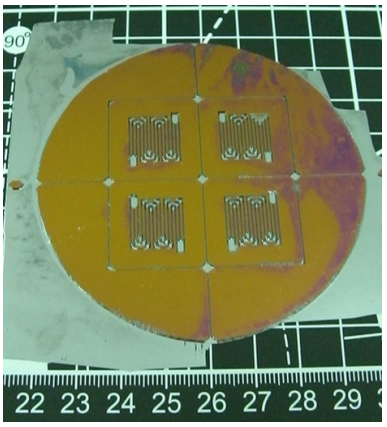

Fig. 3 Silicon substrate after etching process

3 Results and discussion

The results of our numerical simulations were validated with experimental data, and the governing equations were solved using CFD-ACE+ to obtain the polarization curves. The experimental micro PEMFC using MEMS technology was based on a silicon substrate. A single micro PEMFC is assembled to obtain the polarization curve. Two different fuel flow rates were compared in this investigation. The polarization curves of hydrogen and oxygen were supplied at base operating conditions of fuel flow rates of 15 cm^3/min and 40 cm^3/min, respectively, as shown in Figs. 4 and 5.

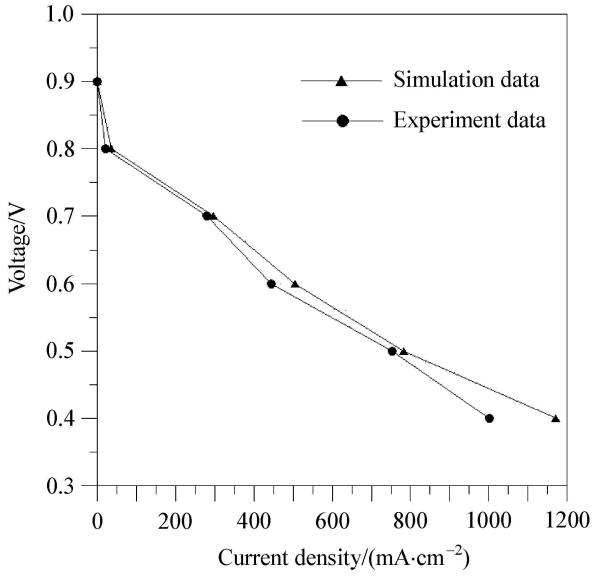

Fig. 4 Comparison of simulation with experiment polarization curves (fuel flow rate at 15 cm^3/min)

The relative difference of the current densities in the numerical data is better than that of the experimental data. Since the effect of water flooding was neglected in the simulation of the cathode side in a single phase model, the numerical values appear to be over-predicted. This explains why

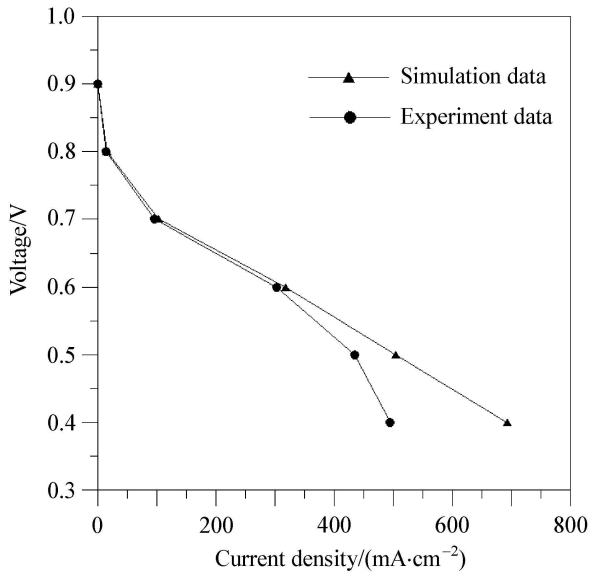

Fig. 5 Comparison of simulation with experiment polarization curves (fuel flow rate at 40 cm^3/min)

the numerical data are better than the experimental ones. However, the simulation results help to elucidate the phenomena observed in the micro PEMFC.

When the fuel flow rate of H_2/O_2 was provided at 15 cm^3/min, the current density was 1 170 mA/cm^2 at 0.4 V in the simulation. When the fuel flow rate was provided at 40 cm^3/min, the current density was 693 mA/cm^2 at 0.4 V. Figure 6 shows two polarization curves for each fuel flow rate. The experiment was performed at ambient pressure and temperature. Pure humidified hydrogen and dry oxygen are fed into the micro PEMFC. As the fuel flow rate increases, the cell performance worsened. Increasing the fuel temperature accelerated the electrochemical reactions and increased the amount of liquid water produced. The decreasing of performance from the experimental results indicate that increasing the gas flow rate will easily degrade the humidity of MEA in a cathode and the diffusion of the gas; besides, it will carries away the heat generated by the micro fuel cell more easily. Thus, internal flooding was not obvious. A low fuel flow rate yielded better performance than that obtained with high fuel flow rates.

These experimental results indicate that the fuel flow rate markedly affects cell performance. However, a high fuel flow rate dries out the membrane, which increases electrical resistance. A fuel flow rate of 15 cm^3/min generates the worst performance.

Figure 7 shows the polarization curves for the two fuel flow rates. The results indicate that low fuel flow rates have higher limiting current densities, around half, compared with high fuel flow rates. This result demonstrates that the output current density is dictated by fuel flow rates, and a superior performance is achieved when applying a low fuel flow rate relative to the fuel permeability in the membrane. Low fuel flow rates enable more fuel to permeate into the membrane and increase cell electrochemical reaction. Thus, a low fuel flow rate provides the ideal performance for the fuel cell. In addition, the temperature and water distributions of the membrane also affect micro fuel cell performance.

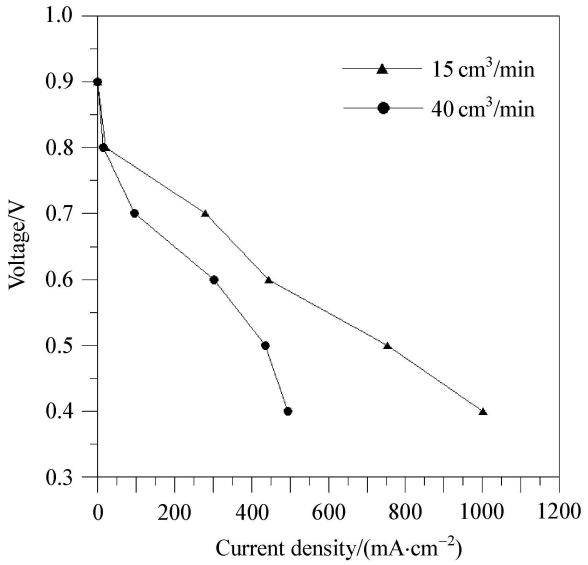

Fig. 6 Comparison of fuel flow rate polarization curves of experiment data

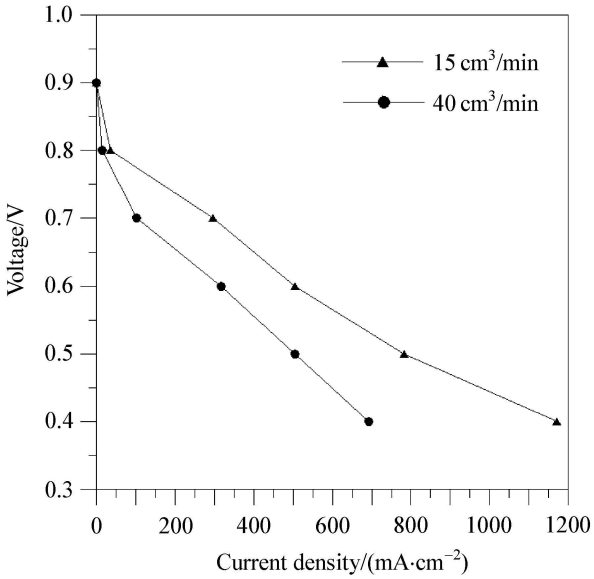

Fig. 7 Comparison of fuel flow rate polarization curves of simulation data

Figure 8 shows the distributions of the local current density in the membrane at an operation voltage of 0.4 V at fuel flow rates of 15 cm^3/min and 40 cm^3/min. For overall current density distributions, the local current density increased from the inlet toward the outlet, leading to a low temperature distribution. The local current density distributions

relative to the temperature are shown in Figs. 9. The results show that uniform temperature distributions (Fig. 9a) lead to a higher current density (Fig. 8a) because the higher fuel permeability enables fuel to reach the membrane faster and enhances the electrochemical reaction. Moreover, a more uniform temperature distribution in micro PEMFC provides lower proton conduction resistance and a more active electrochemical reaction from midstream to downstream along the flow channels. The phenomenon of a gradually increasing local current density distribution appears to be significant from the midstream to downstream. This leads to uniformity of the temperature distribution as well as an increase in the cell current density. In this regard, we used a micro PEMFC that had a small dimension of MEA (only 2.5 cm^2) in this study. Owing to this, the worst performance caused by higher fuel flow rates could result in an increase in hot spots in the membrane that can damage the membrane structure. Consequently, a uniform temperature distribution is important to membrane proton conductivity and an increase in cell performance. This is verified by the experimental results in Fig. 6.

The uniformity of temperature distribution is important for minimizing the material stresses on MEA so that its lifetime could be extended. We tried to discover how the inside temperature of a micro PEMFC is affected by electrochemical reaction. The temperature distributions in the membrane surface of the micro PEMFC at the nominal operating condition, 0.4 V, are shown in Fig. 9. Figure 9 displays the distributions of temperature in the membrane at fuel flow rates of 15 cm^3/min and 40 cm^3/min. Figure 9a shows a more uniform temperature distribution in the membrane at a fuel flow rate of 15 cm^3/min. The temperature slightly decreased with an increase in the current density because the higher electrochemical reaction rate can produce more water, thus wetting the membrane and increasing proton conduction. An enhanced cell performance is observed. The simulations showed in Fig. 9b illustrate a high and non-uniform temperature distribution in the membrane at a fuel flow rate of 40 cm^3/min. The temperature approaches 360 K from the inlet region to the midstream of the membrane, and then drops to around 350 K along the flow path. High temperatures may dry the membrane and increase proton conduction resistance. The lowest temperature is distributed in the middle of the flow channels. This could be due to the existence of low temperatures, as a result of water accumulation, at the exit region. We thus find that the uniformity of temperature distribution indeed influences the electrochemical reaction rate. Low fuel flow rates can cause uniform temperature distributions, from which we can obtain a better micro PEMFC performance.

Water management also affects the performance of micro PEMFCs. To study the effects of water distribution on a micro PEMFC, Fig. 10 presents the water distribution in the membrane at an operation voltage of 0.4 V at fuel flow rates of 15 cm^3/min and 40 cm^3/min. At a fixed overpotential, the water concentration increased from the inlet to the outlet. The results show that a lower fuel flow rate can

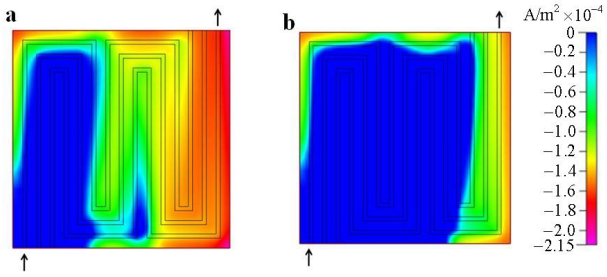

Fig. 8 Distributions of current density in the membrane at operation voltage 0.4 V: **a** Fuel flow rates at 15 cm^3/min; **b** Fuel flow rates at 40 cm^3/min

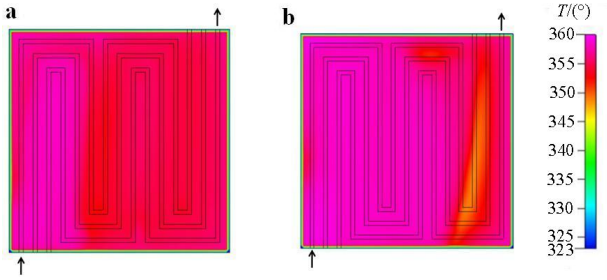

Fig. 9 Distributions of temperature in the membrane at operation voltage 0.4 V: **a** Fuel flow rates at 15 cm^3/min; **b** Fuel flow rates at 40 cm^3/min

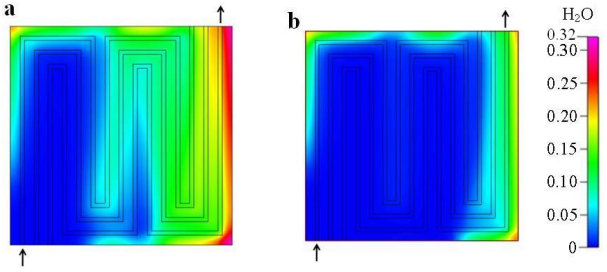

Fig. 10 Distributions of water in the membrane at operation voltage 0.4 V: **a** Fuel flow rates at 15 cm^3/min; **b** Fuel flow rates at 40 cm^3/min

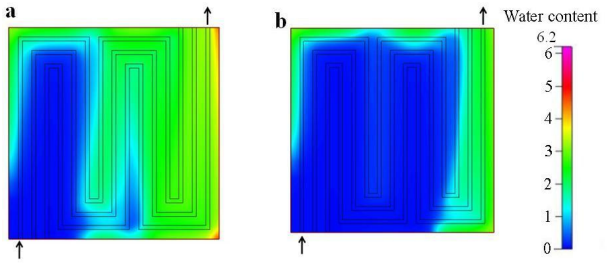

Fig. 11 Distributions of water content in the membrane at operation voltage 0.4 V: **a** Fuel flow rates at 15 cm^3/min; **b** Fuel flow rates at 40 cm^3/min

increase the electrochemical reaction and the quantity of water produced. The results also indicate that the concentration of water is at a maximum at the outlet gas channel region adjacent to the membrane because the consumption of oxygen produces water via an electrochemical reaction. The oxygen concentration is the lowest in this region. When the water diffuses backward from the membrane to the gas channel, water accumulates in the outlet gas channel. The higher fuel flow rate results in a more rapid exhaustion of water. Less water accumulates as the flow rate is increased, implying that a higher proton conduction resistance leads to worse cell performance.

Water content is given as the ratio of the number of water molecules to that of charge ($SO_3^-H^+$) sites. This ratio indicates how well the membrane is hydrated and is the key to reducing membrane electrical resistance. Furthermore, maintaining a uniform distribution of membrane water content can extend the micro PEMFC lifetime because the uniform distribution reduces the formation of local hot spots and flooding that stress and damage the MEA. Figure 11 shows the distributions of water content in the membrane at an operation voltage of 0.4 V at fuel flow rates of 15 cm^3/min and 40 cm^3/min. The membrane water content in this study was lower than 6 since no liquid water was formed. The results show that the current density increased, and the membrane water content also increased for these two different fuel flow rates. The results also found that a higher water content occurred when the fuel flow rate was 15 cm^3/min. This may be due to the gradual increase in current density distributions compared with that found with a fuel flow rate of 40 cm^3/min. The membrane water content in the fuel flow rate of 15 cm^3/min reached 2–5 from the midstream to the downstream of the flow channels. The water content for the cell with a fuel flow rate of 40 cm^3/min only reached 0–3 in all flow channels. These results suggest that the water content distribution is based on a fuel reaction utilizing rate. The cell with a fuel flow rate of 15 cm^3/min has a higher membrane water content at 0.4 V operating voltage due to the higher water production rate from the electrochemical reaction. The water content is linearly related to the proton conductivity such that a higher membrane water content leads to high proton conductivities. This decreases the overpotential caused by ohmic loss. Thus, the micro PEMFC performance is improved.

4 Conclusions

Portable consumer electronic products require a small, lightweight power supply with high capacity. The micro PEMFC satisfies these requirements. The current study employs MEMS technology to etch flow fields on a silicon substrate. The reaction area of this single micro PEMFC is 2.5 cm^2. A single micro PEMFC was successfully fabricated, and its performance was analyzed with a 3-D mathematical model. The model simulates temperature, current density, and water distributions at two different fuel flow rates. The simulation results show that a low and uniform temperature distribution in the membrane at low fuel flow rates can increase membrane water distribution and increase micro PEMFC performance.

Acknowledgments The authors would like to thank National Science Council for financially supporting this research under Contract No. NSC98-2221-E-009-162. Nano Device Laboratories, Center for High-performance Computing, Center for Nanotechnology Research Center in Chiao-Tung University are also commended for fabrication and measurement support.

References

1 Lee, S.J., Cha, S.W., Liu, Y., et al.: High power-density polymer-electrolyte fuel cells by microfabrication. Electrochem Soc. Proceedings (2000)
2 Hsieh, S.S., Kuo, J.K., Hwang, C.F., et al.: A novel design and microfabrication for a micro PEMFC. Microsyst Technol. **10**, 121–126 (2004)
3 Hsieh, S.S., Hwang, C.F., Kuo, J.K., et al.: SU-8 flow field plates for a micro PEMFC. J. Solid State Electrochem **9**, 121–131 (2005)
4 Cha, S.W. O'Hayre, R., Park, Y.I., et al.: Electrochemical impedance investigation of flooding in micro-flow channels for proton exchange membrane fuel cells. J. Power Sources **161**, 138–142 (2006)
5 Hsieh, S.S., Yang, S.H., Feng, C.L.: Characterization of the operational parameters of a H_2/air micro PEMFC with different flow fields by impedance spectroscopy. J. Power Sources **162**, 262–270 (2006)
6 Hsieh, S.S., Feng, C.L., Huang, C.F.: Development and performance analysis of a H_2/air micro PEM fuel cell stack. J. Power Sources **163**, 440–449 (2006)
7 Chiang, M.S., Chu, H.S.: Numerical investigation of transport component design effect on a proton exchange membrane fuel cell. J. Power Sources **160**, 340–352 (2006)
8 Shimpalee, S., Van, Zee J.W.: Numerical studies on rib& channel dimension of flow-field on PEMFC performance. Int. J. Hydrogen Energ. **13**, 842–856 (2007)
9 Matamoros, L., Bruggemann, D.: Numerical study on PEMFC's geometrical parameters under different humidifying conditions. J. Power Sources **172**, 253–264 (2007)
10 Shimpalee, S., Greenway, S., Van, Zee J.W.: The impact of channel length on PEMFC flow-field design. J. Power Sources **160**, 398–406 (2006)
11 Liu, X., Tao, W., Li, Z., et al.: Three-dimensional transport model of PEM fuel cell with straight flow channels. J. Power Sources **158**, 25–35 (2006)
12 Mazumder, S., Cole, J.V.: Rigorous 3-D mathematical modeling of PEM fuel cells II. Model Predictions with Liquid Water Transport. J. Electrochem. Soc. **150**, 1510–1517 (2003)
13 Springer, T.E., Zawodzinski, T.A., Gottesfeld, S.: Polymer electrolyte fuel cell model. J. Electrochem. Soc. **138**, 2334–2342 (1991)